Received: 12 December 2021 | Revised: 23 February 2022 | Accepted: 24 March 2022

DOI: 10.1111/jace.18482

Journal of the American Ceramic Society

SPECIAL ISSUE ARTICLE

Boosting intermediate temperature performance of solid oxide fuel cells via a tri-layer ceria–zirconia–ceria electrolyte

Jun Zhang[1] | **Christian Lenser**[1] | **Niklas Russner**[2] | **André Weber**[2] | **Norbert H. Menzler**[1,3] | **Olivier Guillon**[1,4]

[1]Institute of Energy and Climate Research (IEK), IEK-1: Materials Synthesis and Processing, Forschungszentrum Jülich GmbH, Jülich, Germany

[2]Institute for Applied Materials – Electrochemical Technologies (IAM-ET), Karlsruhe Institute of Technology, Karlsruhe, Germany

[3]Institute of Mineral Engineering (GHI), RWTH Aachen University, Aachen, Germany

[4]Jülich Aachen Research Alliance: JARA-Energy, Jülich, Germany

Correspondence
Christian Lenser, Institute of Energy and Climate Research (IEK), IEK-1: Materials Synthesis and Processing, Forschungszentrum Jülich GmbH, 52425 Jülich, Germany.
Email: c.lenser@fz-juelich.de

Current address
Jun Zhang, Department of Energy Conversion and Storage, Technical University of Denmark, 2800 Kongens Lyngby, Denmark

Funding information
China Scholarship Council, Grant/Award Number: 201606460053; Deutsche Forschungsgemeinschaft (DFG), Grant/Award Number: 491111487

Abstract

Using cost-effective fabrication methods to manufacture a high-performance solid oxide fuel cell (SOFC) is helpful to enhance the commercial viability. Here, we report an anode-supported SOFC with a three-layer $Gd_{0.1}Ce_{0.9}O_{1.95}$ (gadolinia-doped-ceria [GDC])/$Y_{0.148}Zr_{0.852}O_{1.926}$ (8YSZ)/GDC electrolyte system. The first dense GDC electrolyte is fabricated by co-sintering a thin, screen-printed GDC layer with the anode support (NiO–8YSZ substrate and NiO–GDC anode) at 1400°C for 5 h. Subsequently, two electrolyte layers are deposited via physical vapor deposition. The total electrolyte thickness is less than 5 μm in an area of 5 × 5 cm^2, enabling an area-specific ohmic resistance as low as 0.125 Ω cm^{-2} at 500°C (under open circuit voltage), and contributing to a power density as high as 1.2 W cm^{-2} at 650°C (at an operating cell voltage of 0.7 V, using humidified [10 vol.% H_2O] H_2 as fuel and air as oxidant). This work provides an effective strategy and shows the great potential of using GDC as an electrolyte for high-performance SOFC at intermediate temperature.

KEYWORDS
ceria electrolyte, intermediate temperature SOFC, screen printing

1 | INTRODUCTION

Solid oxide fuel cells (SOFCs) face the challenge of maintaining low area specific resistance (ASR) at reduced temperatures as the electrochemical processes taking place in the cell are thermally activated. Focusing on the electrolyte for the present work, the ASR of the electrolyte (ASR_{el}) can be described by its thickness L and material conductivity σ at given temperature: $ASR_{el} = L \cdot \sigma^{-1}$. Thus, the effective strategies to decrease the ASR_{el} are to fabricate a thin electrolyte layer and/or apply a high conductivity material.[1,2]

Gadolinia-doped ceria (GDC) is a well-known fast oxygen ion conducting material with a conductivity around 5×10^{-3} S cm^{-1} at 500°C,[3,4] permitting a layer with a

thickness above 5 μm to satisfy the ASR_{el} = 0.1 Ω cm^{-2} requirement.[5] The main drawback of this material for the application as an electrolyte is the limited oxygen partial pressure (p_{O_2}) range of the electrolytic domain. Doped ceria shows mixed ionic and electronic conduction behavior under reducing atmosphere,[4,6] resulting in a deleterious current leakage that critically reduces the cell efficiency by a deviation of the cell voltage from the Nernst voltage. The reduced voltage is due to an internal short circuit, where the voltage deviation is $\Delta V = I_{el} \cdot R_{el}$, with I_{el} and R_{el} being the electronic current through and resistance of the electrolyte, respectively. Although it is found that the problem of current leakage decreases with decreasing temperature[6] and increasing thickness,[7] the reduced cell voltage is still observed even at a temperature of 450–550°C[8,9] and a thickness of 20–40 μm.[7,9] Moreover, a thick electrolyte inevitably increases the ASR_{el}.

Therefore, a more effective approach to circumvent the short-circuit issue of GDC under reducing conditions is to use a pure oxygen ion-conducting YSZ layer to block the electron conduction, so-called bi-layer electrolyte strategy.[10–12] Taking one specific example here, the open circuit voltage (OCV) of an SOFC with a GDC electrolyte was substantially increased from 0.6 V to near 1.1 V—the Nernst voltage value—using a YSZ (200 nm)/GDC (1 μm) bilayer electrolyte, accompanied with a peak power density increase from 0.38 to over 1 W cm^{-2} at 600°C (gas condition: air and 97% H_2 with 3% H_2O).[12] However, such a YSZ/GDC bi-layer electrolyte naturally increases the ASR_{el} compared to the YSZ single-layer electrolyte (assuming the same YSZ thickness),[13] unless the YSZ can be fabricated much thinner, as thin as a sub-micrometer scale.[10]

In addition to the bilayer strategy, a tri-layer electrolyte system consisting of a GDC layer on the anode side, a YSZ electron-blocking layer in the middle and a second GDC buffer layer on the cathode side was proposed.[14–16] In this configuration, fabrication is simplified by enabling the deposition of a thicker GDC layer to ensure gas tightness, followed by a thin YSZ layer that interdicts the leakage current. The final GDC layer is typically necessary to ensure compatibility with high-performance air electrodes.[17–19] However, as proof-of-concept, both groups used physical vapor deposition (PVD) techniques to deposit all functional layers, from anode to cathode.

In this study, we further explore the potential of such tri-layer electrolyte system by combining the more scalable ceramic powder processing technique screen printing[20,21] with magnetron sputtering.[22] The first GDC layer is fabricated by screen printing on a 5 × 5-cm^2 anode substrate with a thin anode layer, and the half-cell is subsequently co-sintered to ensure a gas-tight electrolyte. Another key advantage is the ability to integrate an Ni–GDC anode (which additionally offers higher performance and stability than Ni/YSZ[3,23]) in the cell, which is a major challenge when using a zirconia-based electrolyte during co-sintering. The subsequent YSZ and GDC layers are fabricated by sputtering to avoid the chemical interdiffusion between YSZ and GDC.[24,25] The methods demonstrated here can be adapted to a large-scale and highly automated fabrication of high-performance SOFC.

2 | EXPERIMENTAL METHODS

2.1 | Screen printing paste synthesis

All the chemicals used for the electrolyte screen printing paste synthesis are commercially available, with their supplier information listed in Table S1. The paste was synthesized in two steps. First, GDC powder (as ordered, without treatment), terpineol, and dispersant with a weight ratio of 64:33:3 (an optimized ratio to achieve the highest solid content in the paste and optimized viscosity for screen printing) were thoroughly mixed in a tumbling mixer (Turbula T2F, Willy A. Bachofen, Uster, Switzerland) at a speed of 72 rpm for 24 h to get a homogeneous pre-suspension. Next, a mixture of ethyl cellulose and terpineol with a weight ratio of 15:85 was added to the pre-suspension with a weight ratio of 20:80 and then mixed in a planetary vacuum mixer (ARV-310CE, THINKY Corporation, Japan) at a speed of 1400 rpm for 2 min to obtain the final screen-printing paste.

2.2 | Tri-layer electrolyte fabrication

A 5 × 5-cm^2 anode support consisting of a highly porous NiO/8YSZ (weight ratio of 60:40) substrate (~0.5 mm) and a microporous NiO/GDC (weight ratio of 50:50) function layer (~7 μm) established in Forschungszentrum Jülich was used.[26] The first GDC layer was fabricated by screen printing the synthesized paste on the support using a semi-automatic screen printer (X1, EKRA, Germany). After drying in the dryer at 60°C for 2 h, the screen-printed layer was then co-sintered with the anode support at 1400°C (with a heating and cooling rate of 3 K min^{-1}) for 5 h to fully densify the first GDC layer. The second YSZ and third GDC layers were fabricated by PVD using a commercial CS 400 ES cluster system (Von Ardenne Anlagentechnik GmbH, Germany). The commercial YSZ ($Y_{0.148}Zr_{0.852}O_{1.926}$, Tosoh, Japan) and GDC ($Gd_{0.1}Ce_{0.9}O_{1.95}$, Fuelcellmaterials, USA) powders were uniaxial-statically pressed and then sintered at 1500°C for 5 h in air to yield PVD targets. Prior to the PVD coating, the fully sintered GDC electrolyte surface was first cleaned using organic solvents (acetone, ethanol, and deionized water mixture) in ultrasonic bath, followed by a sputtering etching (0.7 W cm^{-2}, 1200 s) to condi-

tion the surface. Specifically, electron beam physical vapor deposition was used for YSZ electron blocking layer fabrication and reactive magnetron sputtering for the GDC barrier layer. The sample was heated to 800°C with a ramp rate of 5 K min^{-1}, whereas the deposition time and bias power were adjusted to reach the desired thickness and density of each PVD layer.

2.3 | Electrochemical characterization

For the single-cell performance test, an $La_{0.58}Sr_{0.4}CoO_{3-\delta}$ (LSC) cathode was used. The LSC cathode layer, with a size of 1 × 1 cm^2, was screen printed on the half-cell and sintered at 850°C for 3 h with a heating rate of 3 K min^{-1}. Prior to the cell test, the cell was first reduced at 800°C increasing the H_2 amount in an H_2/N_2 fuel gas mixture in a well-defined reduction procedure. The details of the single-cell measurement setup have been described previously.[27] The *IV*-characteristics were measured from 800 to 400°C. On the cathode side, ambient air was used and H_2 with a humidity of 12% H_2O was fed to the fuel side. The electrochemical impedance spectra (EIS) were collected under open circuit voltage conditions with 10-mV AC amplitude in the range from 1 MHz to 0.03 Hz using a Solartron 1260 frequency response analyzer. A total of three cells were tested, with very good reproducibility.

2.4 | Microstructure characterization

The microstructure investigations were conducted by using scanning electron microscopy (SEM) (ZEISS ULTRA 55, Oberkochen, Germany). The sample preparation was done by grinding with SiC sandpaper of different grid sizes and polishing with a diamond paste of particle size from 3 μm to sub-micrometer.

3 | RESULTS AND DISCUSSION

3.1 | Microstructure

Figure 1A shows a typical cross-sectional SEM microstructure of a half-cell with a macro-porous Ni–YSZ substrate, a finer Ni–GDC anode, and a dense GDC electrolyte layer. After co-sintering with the anode at 1400°C for 5 h, a continuous and homogeneous GDC layer was formed on the anode. The detailed SEM observation of the electrolyte layer (Figure 1B) shows a highly dense microstructure (which is further confirmed by the air leakage rate test in Figure S1) and yields an estimated thickness around 4 μm. As the same material (GDC) is used in both the electrolyte and the anode composite, the electrolyte is well connected to the anode at the interface, providing good mechanical stability. The top view of the screen-printed electrolyte surface after sintering (Figure 1C) shows a dense and smooth surface morphology, particularly favorable for the sub-micrometer-scale thin-film fabrication by PVD.[14,28] This is illustrated in Figure 1D, where two continuous and dense YSZ (light blue bar) and GDC (dark blue bar) layers with thickness around 800 and 600 nm were achieved via PVD on the screen-printed electrolyte surface (note: Figure 1D shows the fuel electrode in the reduced state).

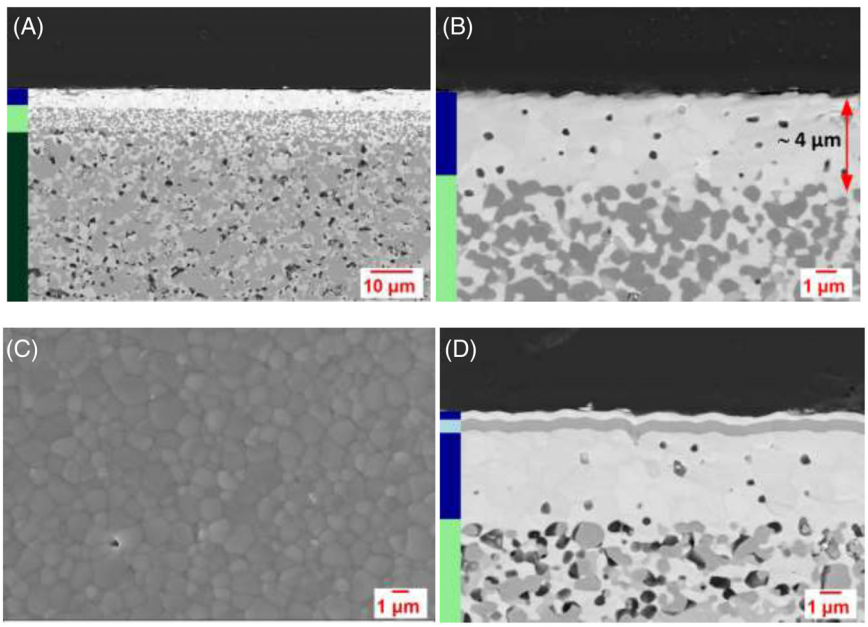

FIGURE 1 SEM images of (A) cross-sectional structure of the half-cell with the screen-printed GDC electrolyte layer after sintering at 1400°C for 5 h, (B) cross-sectional structure of the screen-printed electrolyte layer, (C) surface morphology of the screen-printed electrolyte layer after sintering, and (D) cross-sectional structure of the half-cell after the PVD deposition of YSZ and GDC layers (with colored bar representing different components: dark green—substrate; light green—anode; dark blue—GDC electrolyte; light blue—YSZ electrolyte). (A), (B), and (D) are operated in BSD mode, whereas (C) is operated in in-lens SE mode. BSD, backscattered electron detector; PVD, physical vapor deposition; SE, secondary electron; SEM, scanning electron microscopy

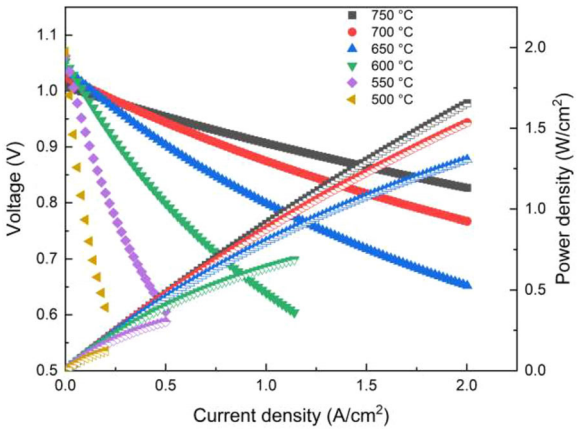

FIGURE 2 Cell voltage (closed symbol) and power density (half-closed symbol) as a function of current density operated from 750 to 500°C, ambient air and humidified H_2 (with 12 vol.% H_2O) were used

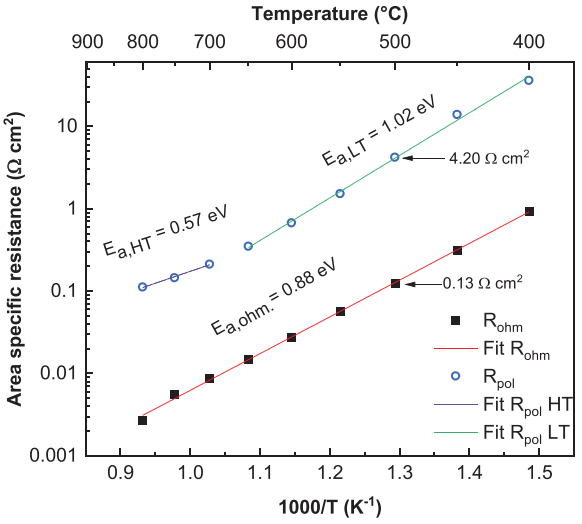

FIGURE 3 Ohmic (R_{ohm}) and electrode polarization resistance (R_{pol}) comparison as a function of temperature (the related Nyquist plots and DRTs are shown in Figure S2). DRT, DRT, distribution of relaxation time

3.2 | Single-cell performance

Figure 2 compares the voltage (v) and power density (P) dependence on current density (i) measured at different temperatures. The OCVs from 750 to 500°C are 1.01, 1.03, 1.04, 1.05, 1.06 and 1.07 V, respectively, corresponding to a relative humidity in the fuel gas around 22% ± 2% at each temperature. The difference to the nominal humidity is most likely due to gas leakage through the electrolyte, possibly a warpage of the cell that hinders a gastight integration in the cell housing, or residual electronic leakage current through the electrolyte. Although such leakage is not desirable, the investigated cells are prototypes and efforts to improve the leakage rate are currently underway. However, the measured power densities are exceptionally high, reaching 1.68 W cm^{-2} at 750°C and 1.31 W cm^{-2} at 650°C for a current density of 2 A cm^{-2}, which are higher than most state-of-the-art SOFCs with thin-film electrolytes or even comparable with the faster-ion-conducting proton conductors (seen in the detailed comparison in Table S2). However, with temperatures below 650°C, the resistance ($\Delta v/\Delta i$) increases quickly, indicating a high activation energy of the dominant processes, probably in the electrode, which will be further investigated in the impedance measurement.

The typical Nyquist plots of the EIS for the cell measured at different temperatures under OCV are compared in Figure S2A. In the plot, the high-frequency intercept on the real axis is assumed to be the ohmic resistance (R_{ohm}) mainly from the oxygen ion conduction through the electrolyte, whereas the difference between the low- and high-frequency intercept is the polarization resistance from the electrodes (R_{pol}). It clearly shows that R_{pol} dominates the overall resistance of the cell at OCV, suggesting that the thin electrolyte effectively reduces R_{ohm}, particularly at low temperatures. Specifically, the corresponding ASR_{ohm} at 650, 600, 550 and 500°C was 0.01, 0.03, 0.06 and 0.13 Ω cm^{-2}, respectively. These values are much lower compared to the 1-μm thick YSZ and even lower than a 5-μm $BaCe_{0.55}Zr_{0.3}Y_{0.15}O_{3-\delta}$ (BZCY) proton-conducting electrolyte (which is favored as low temperature application due to its high proton conductivity), Table S2. The measured ASR_{ohm} for our cell also agrees with the values expected from the given thickness and conductivity values of YSZ and GDC at specific temperature. For example, at 500°C, the corresponding conductivity values of YSZ (~1 × 10^{-3} S cm^{-1}) and GDC (~6 × 10^{-3} S cm^{-1})[5] give a total theoretical ASR of ~0.1 Ω cm^{-2}, closely matching the measured ohmic resistance value (~0.13 Ω cm^{-2}) here. In short, the exceptionally low ASR_{ohm} obtained for our tri-layer electrolyte demonstrates its superiority over the challenging-to-fabricate thin YSZ.

Figure 3 compares the dependence of ohmic (R_{ohm}) and electrode polarization resistances (R_{pol}) on temperature shown in the form of an Arrhenius plot. Although the ohmic contribution can be fitted with a linear function across the entire temperature range (yielding an activation energy of E_A = 0.88 eV), the polarization resistance is clearly not well described with a single activation energy across the entire temperature range. When fitting a high-(700–800°C) and a low-temperature (400–650°C) line, the activation energies of E_A = 0.57 and 1.02 eV are obtained, respectively. This behavior is very similar to that described by Riegraf et al. for Ni–GDC electrodes, although the origin of the different slopes is still

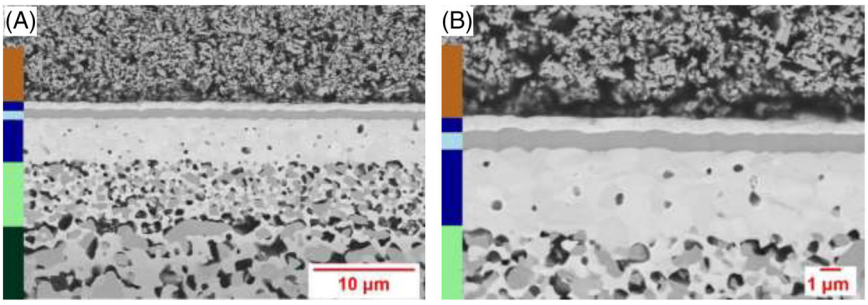

FIGURE 4 Polished cross-sectional BSD SEM images of (A) the full cell structure, and (B) the enlarged electrolyte structure as well as its interfaces with the electrodes, after single-cell test (with colored bar representing different components: dark green—substrate; light green—anode; dark blue—GDC electrolyte; light blue—YSZ electrolyte; light brown—cathode). BSD, backscattered electron detector; SEM, scanning electron microscopy

under debate.[29] However, the similarity indicates that the electrode response is dominated by the Ni–GDC electrode, although the investigated cells in our work have additional gas diffusion impedance from the support that overlaps with the impedance of the Ni–GDC anode. As can be seen in the distribution of relaxation time in Figure S2, the peak at the lowest frequency shows clear temperature dependence, meaning that gas diffusion in the support (which shows hardly any temperature dependence) is not the only cause of this peak. In comparison, the LSC electrode plays a negligible role. This is confirmed by comparing the polarization values to those published for the same LSC cathodes, which are typically one order of magnitude smaller than the obtained polarization resistances of the investigated cell at all temperatures.[30] Therefore, even without a detailed analysis of the impedance spectrum (which is a work in progress), there is strong evidence that the electrode polarization of the investigated cell is strongly dominated by the Ni–GDC electrode.

As a side note, the activation energy of the ohmic resistance indicates that the ohmic resistance is dominated or at least heavily influenced by the YSZ layer, as the obtained value of $E_A = 0.88$ eV is surprisingly high for GDC and more characteristic of YSZ. This is not unexpected, as the GDC layer is approximately 6–8 times thicker than the YSZ layer, which is very close to the ratio of the respective material conductivities at this temperature (see previously mentioned text). Further improvement of the electrolyte ASR can therefore be obtained from reducing the YSZ thickness rather than the GDC thickness.

3.3 | Microstructure analysis after cell test

Figure 4 shows the SEM microstructure observed after the single-cell performance test. The cell maintains its original integrated structure for all the functional layers after cell test, with no obvious delamination or cracks found (Figure 4A). The anode becomes highly porous due to the complete reduction of NiO. In a more focused observation (Figure 4B), we can see a tight adherence of the LSC cathode layer to the GDC electrolyte layer, indicating no detrimental effects of the mismatch of the coefficient of thermal expansion of both materials (LSC: $\sim 20 \times 10^{-6}$ K^{-1},[31] GDC: $\sim 12 \times 10^{-6}$ K^{-1}). Though a slight deformation of GDC should be expected due to its partial reduction under reducing atmosphere, the tri-layer electrolyte keeps its original dense and flat structure. A detailed investigation of the mechanical stresses in the cell under different conditions is currently in progress. In brief, despite the very thin thickness, the electrolyte fabricated in this work has sufficient mechanical stability.

4 | CONCLUSIONS

In summary, we developed a high-performance LT-SOFC with the implementation of a tri-layer ceria–zirconia–ceria electrolyte system, using screen printing and sputtering. Although GDC by itself is not favored for electrolyte applications for intermediate temperature SOFC due to its mixed electronic and ionic conduction behavior and YSZ is challenging to be fabricated in a sub-micrometer scale, we successfully overcome these obstacles by integrating the use of screen printing a ~4-μm dense GDC electrolyte layer (with an area of 5×5 cm^2) and physical vapor depositing a ~800-nm YSZ electron blocking layer atop. Correspondingly, the overall electrolyte resistance is only ~0.01 Ω cm^{-2} at 650°C (and ~0.13 Ω cm^{-2} at 500°C), contributing to a high-performance IT-SOFC with a power density of 1.2 W cm^{-2} operated at 650°C and 0.7 V. Our ability to fabricate such thin, dense, and large area electrolyte layer demonstrated here is easy to be implemented in a large-scale and highly automated way. It is thus meaningful for building high-performance SOFC stacks operated at low temperature. Further work is ongoing to evaluate the long-term stability and investigate cell operation with syngas fuel as well as further simplification of the fabrication processes.

ACKNOWLEDGMENTS

The authors would like to appreciate Frank Vondahlen and Dr. Sven Uhlenbruck (IEK-1 in Forschungszentrum Jülich,

Germany) for their help of the physical vapor deposition, and the partial financial support from China Scholarship Council (CSC No. 201606460053). Open Access funding enabled and organized by Projekt DEAL.

REFERENCES

1. Minh NQ. Ceramic fuel cells. J Am Ceram Soc. 1993;76(3):563–88. https://doi.org/10.1111/j.1151-2916.1993.tb03645.x
2. Kilner JA, Burriel M. Materials for intermediate-temperature solid-oxide fuel cells. Annu Rev Mater Res. 2014;44(1):365–93. https://doi.org/10.1146/annurev-matsci-070813-113426
3. Xia C, Liu M. Microstructures, conductivities, and electrochemical properties of $Ce_{0.9}Gd_{0.1}O_2$ and GDC–Ni anodes for low-temperature SOFCs. Solid State Ionics. 2002;152–153(153):423–30. https://doi.org/10.1016/S0167-2738(02)00381-8
4. Wang S, Kobayashi T, Dokiya M, Hashimoto T. Electrical and ionic conductivity of Gd-doped ceria. J Electrochem Soc. 2000;147(10):3606. https://doi.org/10.1149/1.1393946
5. Zhang J, Lenser C, Menzler NH, Guillon O. Comparison of solid oxide fuel cell (SOFC) electrolyte materials for operation at 500 °C. Solid State Ionics. 2020;344:115138. https://doi.org/10.1016/j.ssi.2019.115138
6. Doshi R, Richards VL, Carter JD, Wang X, Krumpelt M. Development of solid-oxide fuel cells that operate at 500°C. J Electrochem Soc. 1999;146(4):1273–8. https://doi.org/10.1149/1.1391758
7. Duncan KL, Lee K-TT, Wachsman ED. Dependence of open-circuit potential and power density on electrolyte thickness in solid oxide fuel cells with mixed conducting electrolytes. J Power Sources. 2011;196(5):2445–51. https://doi.org/10.1016/j.jpowsour.2010.10.034
8. Lee JG, Park JH, Shul YG. Tailoring gadolinium-doped ceria-based solid oxide fuel cells to achieve 2 W cm^{-2} at 550 °C. Nat Commun. 2014;5(1):4045. https://doi.org/10.1038/ncomms5045
9. Zha S, Moore A, Abernathy H, Liu M. GDC-based low-temperature SOFCs powered by hydrocarbon fuels. J Electrochem Soc. 2004;151(8):A1128. https://doi.org/10.1149/1.1764566
10. Oh EO, Whang CM, Lee YR, Park S-Y, Prasad DH, Yoon KJ, et al. Extremely thin bilayer electrolyte for solid oxide fuel cells (SOFCs) fabricated by chemical solution deposition (CSD). Adv Mater. 2012;24(25):3373–7. https://doi.org/10.1002/adma.201200505
11. Park BK, Barnett SA. Boosting solid oxide fuel cell performance: via electrolyte thickness reduction and cathode infiltration. J Mater Chem A. 2020;8(23):11626–31. https://doi.org/10.1039/d0ta04280c
12. Myung DH, Hong J, Yoon K, Kim B-K, Lee H-W, Lee J-H, et al. The effect of an ultra-thin zirconia blocking layer on the performance of a 1-μm-thick gadolinia-doped ceria electrolyte solid-oxide fuel cell. J Power Sources. 2012;206:91–6. https://doi.org/10.1016/j.jpowsour.2012.01.117
13. Zhang X, Robertson M, Decès-Petit C, Xie Y, Hui R, Yick S, et al. NiO-YSZ cermets supported low temperature solid oxide fuel cells. J Power Sources. 2006;161(1):301–7. https://doi.org/10.1016/j.jpowsour.2006.03.057
14. Noh HS, Hong J, Kim H, Yoon KJ, Lee J-H, Kim B-K, et al. Sandwiched ultra-thin yttria-stabilized zirconia layer to effectively and reliably block reduction of thin-film gadolinia-doped ceria electrolyte. J Ceram Soc Jpn. 2015;123(1436):263–7. https://doi.org/10.2109/jcersj2.123.263
15. Uhlenbruck S, Nédélec R, Sebold D, Buchkremer HP, Stöver D. Electrode and electrolyte layers for solid oxide fuel cells applied by physical vapor deposition (PVD). ECS Trans. 2019;35(1):2275–82. https://doi.org/10.1149/1.3570223
16. Shin SS, Kim JH, Bae KT, Lee K-T, Kim SM, Son J-W, et al. Multiscale structured low-temperature solid oxide fuel cells with 13 W power at 500°C. Energy Environ Sci. 2020;13:3459–68. https://doi.org/10.1039/d0ee00870b
17. Szász J, Wankmüller F, Wilde V, Heike S, Dagmar M, Norbert H, et al. Nature and functionality of $La_{0.58}Sr_{0.4}Co_{0.2}Fe_{0.8}O_{3-\delta}/Gd_{0.2}Ce_{0.8}O_{2-\delta}/Y_{0.16}Zr_{0.84}O_{2-\delta}$ interfaces in SOFCs. J Electrochem Soc. 2018;165(10):F898–906. https://doi.org/10.1149/2.0031811jes
18. Chou J-T, Inoue Y, Kawabata T, Matsuda J, Taniguchi S, Sasaki K. Mechanism of $SrZrO_3$ formation at GDC/YSZ interface of SOFC cathode. J Electrochem Soc. 2018;165(11):F959–65. https://doi.org/10.1149/2.0551811jes
19. Dieterle L, Bockstaller P, Gerthsen D, Hayd J, Ivers-Tiffée E, Guntow U. Microstructure of nanoscaled $La_{0.6}Sr_{0.4}CoO_{3-\delta}$ cathodes for intermediate-temperature solid oxide fuel cells. Adv Energy Mater. 2011;1(2):249–58. https://doi.org/10.1002/aenm.201000036
20. Rotureau D, Viricelle JP, Pijolat C, Caillol N, Pijolat M. Development of a planar SOFC device using screen-printing technology. J Eur Ceram Soc. 2005;25(12 Spec. Iss.):2633–6. https://doi.org/10.1016/j.jeurceramsoc.2005.03.115
21. Ried P, Lorenz C, Brönstrup A, Graule T, Menzler NH, Sitte W, et al. Processing of YSZ screen printing pastes and the characterization of the electrolyte layers for anode supported SOFC. J Eur Ceram Soc. 2008;28(9):1801–8. https://doi.org/10.1016/j.jeurceramsoc.2007.11.018
22. Solovyev AA, Lebedynskiy AM, Shipilova AV, Ionov IV, Smolyansky EA, Lauk AL, et al. Scale-up of solid oxide fuel cells with magnetron sputtered electrolyte. Fuel Cells. 2017;17(3):378–82. https://doi.org/10.1002/fuce.201600227
23. Liu M, van der Kleij A, Verkooijen AHM, Aravind PV. An experimental study of the interaction between tar and SOFCs with Ni/GDC anodes. Appl Energy. 2013;108:149–57. https://doi.org/10.1016/j.apenergy.2013.03.020
24. Lenser C, Jeong H, Sohn YJ, Russner N, Guillon O, Menzler NH. Interaction of a ceria-based anode functional layer with a stabilized zirconia electrolyte: considerations from a materials perspective. J Am Ceram Soc. 2018;101(2):739–48. https://doi.org/10.1111/jace.15214
25. Tsoga A, Gupta A, Naoumidis A, Nikolopoulos P. Gadolinia-doped ceria and yttria stabilized zirconia interfaces: regarding their application for SOFC technology. Acta Mater. 2000;48(18–19):4709–14. https://doi.org/10.1016/S1359-6454(00)00261-5
26. Schafbauer W, Menzler NH, Buchkremer HP. Tape casting of anode supports for solid oxide fuel cells at Forschungszentrum Jülich. Int J Appl Ceram Technol. 2014;11(1):125–35. https://doi.org/10.1111/j.1744-7402.2012.02839.x
27. Timmermann H, Sawady W, Reimert R, Ivers-Tiffée E. Kinetics of (reversible) internal reforming of methane in solid oxide fuel cells under stationary and APU conditions. J Power

Sources. 2010;195(1):214–22. https://doi.org/10.1016/j.jpowsour.2009.07.019

28. Nédélec R, Uhlenbruck S, Sebold D, Haanappel VAC, Buchkremer HP, Stöver D. Dense yttria-stabilised zirconia electrolyte layers for SOFC by reactive magnetron sputtering. J Power Sources. 2012;205:157–63. https://doi.org/10.1016/j.jpowsour.2012.01.054
29. Riegraf M, Dierickx S, Weber A, Costa R, Schiller G, Friedrich KA. Electrochemical impedance analysis of Ni/CGO10-based electrolyte-supported cells. ECS Trans. 2019;91(1):1985–92. https://doi.org/10.1149/09101.1985ecst
30. Lenser C, Zurek J, Naumenko D, Thieu C-A, Son J-W, de Haart U, et al. Performance analysis of a planar solid oxide fuel cell stack between 750°C and 500°C. J Power Sources. 2020;474:228671. https://doi.org/10.1016/j.jpowsour.2020.228671
31. Huang K, Lee HY, Goodenough JB. Sr- and Ni-doped $LaCoO_3$ and $LaFeO_3$ perovskites: new cathode materials for solid-oxide fuel cells. J Electrochem Soc. 1998;145(9):3220–7. https://doi.org/10.1149/1.1838789

SUPPORTING INFORMATION

Additional supporting information may be found in the online version of the article at the publisher's website.

How to cite this article: Zhang J, Lenser C, Russner N, Weber A, Menzler NH, Guillon O. Boosting intermediate temperature performance of solid oxide fuel cells via a tri-layer ceria–zirconia–ceria electrolyte. J Am Ceram Soc. 2023;106:93–99. https://doi.org/10.1111/jace.18482